FED-Vol. 205/AMD-Vol. 190, Developments in
Electrorheological Flows and Measurement Uncertainty
ASME 1994

MAGNETIC FIELD CONTROL OF VORTICITY IN STEADY INCOMPRESSIBLE LAMINAR FLOWS

George S. Dulikravich and Kwang-Yoon Choi
Department of Aerospace Engineering
Pennsylvania State University
University Park, Pennsylvania

Seungsoo Lee
Department of Aerodynamics
Agency for Defense Development
Taejon, Korea

ABSTRACT

A set of highly accurate computer analysis codes for steady multidimensional laminar MHD flows of incompressible fluids with temperature-dependent physical properties has been used to analyze simple MHD flows. In cases of two dimensional flows between parallel plates with a magnetic field of alternating polarity applied orthogonally to the flow direction the result was formation of recirculating regions adjacent to the magnets. In the case of a three-dimensional duct flow with magnetic strips of uniform strength and altering polarity forming the bottom wall a complex pattern of secondary flow was observed. The general trend of the flow is to become tilted towards the magnetic strips and development of narrow regions of high pressure immediately adjacent to the magnets with a wider region of unexpectedly lower pressure immediately above these regions. Predicted distribution of the magnetic field intensities demonstrate that a number of magnetic field lines escape through the inlet and exit boundaries. Implications of such flow patterns, pressure fields and magnetic fields on flow separation control, bubble cloud formation and magnetic signature increase, have been discussed.

NOMENCLATURE

$\mathbf{B}$	= magnetic flux density, T
c	= specific heat, J kg^{-1} K^{-1}
Ec	= Eckert number
Fr	= Froude number
$\mathbf{g}(g_X,g_Y,g_Z)$	= gravity force per unit volume, m s^{-2}
Gr	= Grashof number
$\mathbf{H}(H_X,H_Y,H_Z)$	= magnetic field intensity, H kg^{-1}
H_t	= Hartmann number
$\mathbf{I}$	= unit or identity tensor
k	= heat conductivity coefficient, W m^{-1} K^{-1}
l	= length, m
p	= pressure, kg m^{-1} s^{-2}
P_m	= magnetic Prandtl number
Pr	= Prandtl number
Rm	= magnetic Reynolds number
Re	= hydrodynamic Reynolds number
t	= time, s
T	= absolute temperature, K
ΔT_o	= reference temperature difference, K
v(u,v,w)	= velocity vector, m s^{-1}
x,y,z	= Cartesian coordinates, m
α	= thermal expansion coefficient, K^{-1}
β	= artificial compressibility parameter
μ	= magnetic permeability coefficient, H m^{-1}
η	= viscosity coefficient, kg m^{-1} s^{-1}
ξ, η, ζ	= non-orthogonal grid coordinates
ρ	= fluid density, kg m^{-3}
σ	= electrical conductivity coeff., Ω^{-1} m^{-1}
ϕ	= gravity potential

Subscripts

o	= reference value
cold	= cold wall
hot	= hot wall
i	= component of a vector
j	= component of a vector
,	= differentiation

Superscripts

transp	= transpose of a matrix or a vector
*	= non-dimensional values

INTRODUCTION

It has been well known analytically (Chandrasekhar ,1961; Stuetzer, 1962) and demonstrated computationally (Ozoe and Okada, 1989; Vives 1989; Sterl, 1990; Lee and Dulikravich, 1991) that the electromagnetic fields can influence flow field of an electrically conducting fluid. Our formulation is based on the fundamental concepts of Magneto-Hydro-Dynamics (MHD) as opposed to Electro-Hydro-Dynamics (EHD) (Stuetzer, 1962; Dulikravich, Ahuja and Lee, 1994a; 1994b). In MHD, there are no externally applied electric fields and electrically charged particles in the fluid. The main consequence of applying a magnetic field in MHD is the alteration of vorticity in the flow field depending on the magnetic field orientation and spatial distribution.

Practical applications of the MHD phenomena involve electromagnetic pumping (Seyed-Yagoobi et al., 1989; Ma, Moon and Walker, 1994), magnetized fiber orientation and concentration control during curing of composite materials (Hatta and Yamashita, 1988; Dulikravich, Kosovic and Lee, 1993), control of melt motion during solidification (Dulikravich, Ahuja and Lee, 1994a), stabilization of thin fluid streams in free flow electrophoretic separation (Ivory et al., 1987), and laminarization of submerged jets (Ievlev and Levin, 1989) among many others.

Recently, a group of researchers at Princeton University headed by Daniel Nosenchuk and Garry Brown (1992) announced a significant breakthrough in the ability to use MHD and EHD effects to reduce drag forces that fluids exert on the solid surfaces of the objects like maritime vehicles. Their conclusion was based on the laboratory experiments with a very special arrangement of electrodes and magnets on the surface of a flat plate. The result was reportedly an effective relaminarization of an initially turbulent flow suggesting that it could also be used for flow separation prevention and effective maneuverability of naval vessels without control surfaces The significant commercial implications of this concept, if actually proven, are complemented by equally important military applications. Nevertheless, strong magnetic fields that are anticipated in actual full scale applications will unavoidably create seawater electrolysis (Tempelmeyer, 1990) and consequent bubble noise problem, electrode surface erosion and electromagnetic field signature increase (Jones 1994).

Another group of researchers at Naval Underwater Systems Command headed by Charles Henoch (1994) has been experimenting with MHD control of turbulent boundary layers where magnetic strips and electrodes were intermittently imbedded in a flat surface parallel to the main flow direction. The objective was to create Lorentz forces in the main stream direction thus altering the boundary layer velocity profile and consequently the surface viscous drag. One could also think of segmenting the electrode strips so that each segment of each electrode could be activated independently. This concept has been suggested for enhancement of large scale water purification using electrodialysis by intentionally creating electromembranes that have inhomogeneous electrical conductivities (Mischuk and Dukhin, 1991; Rubinstein, 1991; Dukhin and Mischuk, 1993).

In this paper we intend to examine only one fundamental aspect of the MHD flow control, that is, demonstrate numerically the basic flow patterns, pressure fields and magnetic fields in the case of laminar, steady, incompressible flow of a homogeneous fluid (seawater) through a two-dimensional channel and a three-dimensional duct. We will not attempt to include the effects of seawater electrolysis, consequent bubble cloud formation, and unsteadiness of the flow field. But, we will account for the steady phenomena concerning flowfield and magnetic field signature. Detailed and meaningful effort is needed to follow this initial computational study in order to create an adequate two-phase MHD turbulence model and to appropriately model bubble cloud formation and its dynamics. Hence, our present effort should be understood only as an initial and phenomenological partial proof of the concept that reasonably strong magnetic fields can effectively alter the flow pattern of seawater at low Reynolds numbers.

We will use an extended Boussinesq approximation formulation (Gray and Giorgini, 1976) that allows for arbitrary temperature-dependent density, heat conductivity, specific heat and viscosity of the fluid. We will utilize classical MHD formulation (Stuetzer, 1962) for the governing systems of partial differential equations. Finally, we will use our proven two-dimensional and three-dimensional MHD computer codes (Lee and Dulikravich, 1991; Dulikravich, Ahuja and Lee, 1994a) to simulate flows with spatially varying externally applied magnetic fields. Our formulation simultaneously predicts detailed velocity, pressure, temperature and magnetic fields by using a single computer code. In this work we have formulated the entire problem as three-dimensional and time-dependent, although our computational results will be for steady situations only.

MODELING MHD INCOMPRESSIBLE FLOWS

Since we will be accounting for temperature-dependent physical properties of the fluid, it is convenient to use non-dimensional temperature, $T^* = (T - T_o)/\Delta T$. Here, $\Delta T = T_{hot} - T_{cold}$ and $T_o = T_{cold}$. We will then assume linear variation of density as a function of the non-dimensional temperature so that

$$\rho^* = \frac{\rho}{\rho_o} = 1 + \frac{\partial(\rho/\rho_o)}{\partial T}(T - T_o)$$

$$= 1 + \frac{\partial \rho^*}{\partial T^*}(T^* - T^*_o) = 1 - \alpha^* (T^* - T^*_o) \qquad (1)$$

The partial differential equations governing fluid flow (Navier-Stokes) and the magnetic field intensity transport (Maxwell) can be non-dimensionalized using the following relations (Dulikravich, Ahuja and Lee, 1994a)

$$\mathbf{v}^* = \frac{\mathbf{v}}{|\mathbf{v}_o|} \qquad \mathbf{g}^* = \frac{\mathbf{g}}{|\mathbf{g}_o|} \qquad \mathbf{H}^* = \frac{\mathbf{H}}{|\mathbf{H}_o|} \qquad (2)$$

$$\mathbf{x}^* = \frac{\mathbf{x}}{l_o} \qquad t^* = \frac{t\,|\mathbf{v}_o|}{l_o} \qquad p^* = \frac{p}{\rho_o\,|\mathbf{v}_o|^2} \qquad (3)$$

with η, k and c been arbitrary functions of temperature

$$\eta^* = \frac{\eta}{\eta_o} \qquad k^* = \frac{k}{k_o} \qquad c^* = \frac{c}{c_o} \tag{4}$$

In this work we assumed that α, σ and μ do not vary with temperature, that is,

$$\alpha^* = \frac{\alpha}{\alpha_o} = 1 \qquad \sigma^* = \frac{\sigma}{\sigma_o} = 1 \qquad \mu^* = \frac{\mu}{\mu_o} = 1 \tag{5}$$

Typical non-dimensional numbers used in MHD are

$$Re = \frac{\rho_o \, |v_o| \, l_o}{\eta_o} \qquad Fr^2 = \frac{|v_o|^2}{|g_o| \, l_o} \tag{6}$$

$$Pr = \frac{\eta_o \, c_o}{k_o} \qquad Ec = \frac{|v_o|^2}{c_o \, \Delta T_o} \tag{7}$$

$$P_m = \frac{\mu_o \, \sigma_o \, \eta_o}{\rho_o} \qquad Gr = \frac{\rho_o^2 \, \alpha_o \, |g_o| \, \Delta T_o \, l_o^3}{\eta_o^2} \tag{8}$$

$$H_t = (\mu_o \, |H_o|) \, l_o \left(\frac{\sigma_o}{\eta_o}\right)^{1/2} \qquad R_m = P_m \, R_e \tag{9}$$

The non-dimensional Navier-Stokes equations for MHD flows of homocompositional liquids after implementing extended Boussinesq approximation (Gray and Giorgini, 1976) become:

Mass conservation

$$\nabla^* \cdot \mathbf{v}^* = 0 \tag{10}$$

Linear momentum conservation for MHD flows with magnetic force and thermal buoyancy

$$\frac{\partial \mathbf{v}^*}{\partial t^*} + \nabla^* \cdot (\mathbf{v}^* \, \mathbf{v}^* + \bar{\bar{p}}^* \, \mathbf{I})$$

$$= \frac{1}{Re} \nabla^* \cdot \left(\eta^* \left(\nabla^* \mathbf{v}^* + (\nabla^* \mathbf{v}^*)^{transp}\right)\right)$$

$$+ \frac{H_t^2}{R_m Re} (\nabla^* \times \mathbf{H}^*) \times \mathbf{H}^* + \frac{Gr}{Re^2} \alpha^* (T^* - T_o^*) \, \mathbf{g}^* \tag{11}$$

Here, non-dimensional hydrostatic and hydrodynamic, pressures were combined to give

$$\bar{\bar{p}}^* = \frac{p^*}{\rho^*} + \frac{\phi^*}{Fr^2} \tag{12}$$

where ϕ^* is the non-dimensional gravity potential

$$\mathbf{g}^* = \nabla^* \phi^* \tag{13}$$

Energy conservation for MHD flows including Joule heating

$$c^* \frac{\partial T^*}{\partial t^*} + \nabla^* \cdot (c^* T^* \mathbf{v}^*) = \frac{1}{Re \, Pr} \nabla^* \cdot (k^* \nabla^* T^*)$$

$$+ \frac{H_t^2 \, Ec}{R_m^2 \, Re} (\nabla^* \times \mathbf{H}^*) \cdot (\nabla^* \times \mathbf{H}^*) \tag{14}$$

The magnetic field transport equations for the MHD flow must be solved simultaneously with the preceding augmented Navier-Stokes equation system. The non-dimensional form of the magnetic field intensity (Lee and Dulikravich, 1991) is

$$\frac{\partial \mathbf{H}^*}{\partial t^*} - \nabla^* \times (\mathbf{v}^* \times \mathbf{H}^*) = \frac{1}{R_m} \nabla^* \cdot (\nabla^* \mathbf{H}^*) \tag{15}$$

NUMERICAL MODEL FOR MHD FLOWS

In the case of a general three-dimensional MHD flow, equations 10, 11, 14 and 15 represent a system of eight coupled non-linear partial differential equations. This single system can be split into two interacting systems (Lee and Dulikravich, 1991).

The first system represents the non-dimensional Navier-Stokes equations for incompressible flows with thermal buoyancy and augmented with magnetic field effects. Expressed in a fully conservative form in terms of the non-orthogonal grid-following boundary-fitted coordinate system it becomes

$$\tilde{\mathbf{D}}^{*I}_{NS} \left(\frac{\partial \tilde{\mathbf{Q}}^*_{NS}}{\partial t^*} + \frac{\partial \tilde{\mathbf{E}}^*_{NS}}{\partial \xi^*} + \frac{\partial \tilde{\mathbf{F}}^*_{NS}}{\partial \eta^*} + \frac{\partial \tilde{\mathbf{G}}^*_{NS}}{\partial \zeta^*}\right)$$

$$= \frac{\partial}{\partial \xi^*} \left(\frac{\tilde{\mathbf{D}}^{*v}_{NS}}{J^*} \, g^*_{ij} \, \frac{\partial (J^* \tilde{\mathbf{Q}}^*_{NS})}{\partial \xi^*} \right)$$

$$+ \frac{\partial}{\partial \eta^*} \left(\frac{\tilde{\mathbf{D}}^{*v}_{NS}}{J^*} \, g^*_{ij} \, \frac{\partial (J^* \tilde{\mathbf{Q}}^*_{NS})}{\partial \eta^*} \right)$$

$$+\frac{\partial}{\partial\zeta^*}\left(\frac{\tilde{\mathbf{D}}^{*v}_{NS}}{J^*}\, g^*_{ij}\,\frac{\partial\,(J^*\,\tilde{\mathbf{Q}}^*_{NS})}{\partial\zeta^*}\right)+\tilde{\mathbf{S}}^*_{NS} \qquad (16)$$

Here, $\xi^* = \xi^*(x^*,y^*,z^*)$, $\eta^* = \eta^*(x^*,y^*,z^*)$, $\zeta^* = \zeta^*(x^*,y^*,z^*)$, $\tilde{\mathbf{Q}}^*_{NS}$ is the transformed solution vector, $\tilde{\mathbf{E}}^*_{NS}$, $\tilde{\mathbf{F}}^*_{NS}$ and $\tilde{\mathbf{G}}^*_{NS}$ are the transformed flux vectors, $\tilde{\mathbf{S}}^*_{NS}$ are the transformed source vectors containing influence of magnetic field body forces and Joule heating, and

$$\tilde{\mathbf{D}}^{*I}_{NS} = \mathrm{diag}\left[\,1 \quad 1 \quad 1 \quad 1 \quad c^*\,\right] \qquad (17)$$

$$\tilde{\mathbf{D}}^{*v}_{NS} = \mathrm{diag}\left[0 \quad \frac{\mu^*}{Re} \quad \frac{\mu^*}{Re} \quad \frac{\mu^*}{Re} \quad \frac{k^*}{RePr}\right] \qquad (18)$$

Here, $J^* = 1/\det[(\frac{\partial(x,y,z)}{\partial(\xi,\eta,\zeta)})]$ is the non-dimensional determinant of the Jacobian geometric transformation matrix. The non-dimensional metric tensor components are defined as

$$g^*_{ij} = \frac{\partial\bar{x}_i}{\partial\hat{x}_j}\frac{\partial\bar{x}_j}{\partial\hat{x}_i} \qquad (19)$$

where $\bar{x}_i = \bar{x}_i(x, y, z)$ is the Cartesian coordinate vector and $\hat{x}_i = \hat{x}_i(\xi, \eta, \zeta)$ is the curvilinear coordinate vector. The contravariant components U^*, V^*, W^* and H^*_ξ, H^*_η, H^*_ζ are defined as

$$\begin{Bmatrix} U^* \\ V^* \\ W^* \end{Bmatrix} = \begin{bmatrix} \xi,x & \xi,y & \xi,z \\ \eta,x & \eta,y & \eta,z \\ \zeta,x & \zeta,y & \zeta,z \end{bmatrix} \begin{Bmatrix} u^* \\ v^* \\ w^* \end{Bmatrix} \qquad (20)$$

$$\begin{Bmatrix} H^*_\xi \\ H^*_\eta \\ H^*_\zeta \end{Bmatrix} = \begin{bmatrix} \xi,x & \xi,y & \xi,z \\ \eta,x & \eta,y & \eta,z \\ \zeta,x & \zeta,y & \zeta,z \end{bmatrix} \begin{Bmatrix} H^*_x \\ H^*_y \\ H^*_z \end{Bmatrix} \qquad (21)$$

where subscripts after the comma designate partial differentiation with respect to the variable that follows the comma. For the actual numerical discretization in the computational space having uniform grid ($\Delta\xi = \Delta\eta = \Delta\zeta = 1$) we used

$$\begin{aligned}
\xi,x &= (y,\eta\ z,\zeta - y,\zeta\ z,\eta)\ J^* \\
\xi,y &= (x,\zeta\ z,\eta - x,\eta\ z,\zeta)\ J^* \\
\xi,z &= (x,\eta\ y,\zeta - x,\zeta\ y,\eta)\ J^* \\
\eta,x &= (y,\zeta\ z,\xi - y,\xi\ z,\zeta)\ J^* \\
\eta,y &= (x,\xi\ z,\zeta - x,\zeta\ z,\xi)\ J^* \\
\eta,z &= (x,\zeta\ y,\xi - x,\xi\ y,\zeta)\ J^* \\
\zeta,x &= (y,\xi\ z,\eta - y,\eta\ z,\xi)\ J^* \\
\zeta,y &= (x,\eta\ z,\xi - x,\xi\ z,\eta)\ J^* \\
\zeta,z &= (x,\xi\ y,\eta - x,\eta\ y,\xi)\ J^*
\end{aligned} \qquad (22)$$

An unsteady artificial compressibility term (Chorin, 1967) was added to the mass conservation so that the augmented Navier-Stokes system (16) is not singular and can be integrated simultaneously. The vector of solution variables is given as

$$\tilde{\mathbf{Q}}^*_{NS} = \frac{1}{J^*}\left\{\frac{p^*}{\beta} \quad u^* \quad v^* \quad w^* \quad T^*\right\}^{transp} \qquad (23)$$

Here, β is a user specified parameter with values $1 < \beta < 5$. For sufficiently large number of converging iterations, the time variation of the first term in $\tilde{\mathbf{Q}}^*_{NS}$ approaches zero value and does not influence the accuracy of the steady state solution. Flux vectors in Navier-Stokes equations (16) are,

$$\tilde{E}^*_{NS} = \frac{1}{J^*}\begin{Bmatrix} U^* \\ U^*u^* + \xi_{,x}\,\bar{\bar{p}}^* \\ U^*v^* + \xi_{,y}\,\bar{\bar{p}}^* \\ U^*w^* + \xi_{,z}\,\bar{\bar{p}}^* \\ c^*U^*T^* \end{Bmatrix} \tag{24}$$

$$\tilde{F}^*_{NS} = \frac{1}{J^*}\begin{Bmatrix} V^* \\ V^*u^* + \eta_{,x}\,\bar{\bar{p}}^* \\ V^*v^* + \eta_{,y}\,\bar{\bar{p}}^* \\ V^*w^* + \eta_{,z}\,\bar{\bar{p}}^* \\ c^*V^*T^* \end{Bmatrix} \tag{25}$$

$$\tilde{G}^*_{NS} = \frac{1}{J^*}\begin{Bmatrix} W^* \\ W^*u^* + \zeta_{,x}\,\bar{\bar{p}}^* \\ W^*v^* + \zeta_{,y}\,\bar{\bar{p}}^* \\ W^*w^* + \zeta_{,z}\,\bar{\bar{p}}^* \\ c^*W^*T^* \end{Bmatrix} \tag{26}$$

The non-zero components of the source vector $\tilde{S}^*_{NS}$ are

$$\tilde{S}^*_{NS2} = \frac{H_t^2}{R_m R_e}\left(\frac{\partial}{\partial\xi^*}\left(\frac{H^*\xi H^*x}{J^*}\right) + \frac{\partial}{\partial\eta^*}\left(\frac{H^*\eta H^*x}{J^*}\right) + \frac{\partial}{\partial\zeta^*}\left(\frac{H^*\zeta H^*x}{J^*}\right)\right) - \frac{Gr}{J^* Re^2}\,\alpha^*\,(T^* - T^*_o)\,g^*_x \tag{27}$$

$$\tilde{S}^*_{NS3} = \frac{H_t^2}{R_m R_e}\left(\frac{\partial}{\partial\xi^*}\left(\frac{H^*\xi H^*y}{J^*}\right) + \frac{\partial}{\partial\eta^*}\left(\frac{H^*\eta H^*y}{J^*}\right) + \frac{\partial}{\partial\zeta^*}\left(\frac{H^*\zeta H^*y}{J^*}\right)\right) - \frac{Gr}{J^* Re^2}\,\alpha^*\,(T^* - T^*_o)\,g^*_y \tag{28}$$

$$\tilde{S}^*_{NS4} = \frac{H_t^2}{R_m R_e}\left(\frac{\partial}{\partial\xi^*}\left(\frac{H^*\xi H^*z}{J^*}\right) + \frac{\partial}{\partial\eta^*}\left(\frac{H^*\eta H^*z}{J^*}\right) + \frac{\partial}{\partial\zeta^*}\left(\frac{H^*\zeta H^*z}{J^*}\right)\right) - \frac{Gr}{J^* Re^2}\,\alpha^*\,(T^* - T^*_o)\,g^*_z \tag{29}$$

$$\tilde{S}^*_{NS5} = J^*\frac{H_t^2\,Ec}{R_m^2\,R_e}\left(\tilde{P}^2_{yz} + \tilde{P}^2_{zx} + \tilde{P}^2_{xy}\right) \tag{30}$$

where (Lee and Dulikravich, 1991)

$$\tilde{P}_{yz} = \frac{\partial}{\partial\xi^*}\left(\frac{H^*z\,\xi_{,y} - H^*y\,\xi_{,z}}{J^*}\right) + \frac{\partial}{\partial\eta^*}\left(\frac{H^*z\,\eta_{,y} - H^*y\,\eta_{,z}}{J^*}\right) + \frac{\partial}{\partial\zeta^*}\left(\frac{H^*z\,\zeta_{,y} - H^*y\,\zeta_{,z}}{J^*}\right) \tag{31}$$

$$\tilde{P}_{zx} = \frac{\partial}{\partial\xi^*}\left(\frac{H^*x\,\xi_{,z} - H^*z\,\xi_{,x}}{J^*}\right) + \frac{\partial}{\partial\eta^*}\left(\frac{H^*x\,\eta_{,z} - H^*z\,\eta_{,x}}{J^*}\right) + \frac{\partial}{\partial\zeta^*}\left(\frac{H^*x\,\zeta_{,z} - H^*z\zeta_{,x}}{J^*}\right) \tag{32}$$

$$\tilde{P}_{xy} = \frac{\partial}{\partial\xi^*}\left(\frac{H^*y\,\xi_{,x} - H_x\,\xi_{,y}}{J^*}\right) + \frac{\partial}{\partial\eta^*}\left(\frac{H^*y\,\eta_{,x} - H^*x\,\eta_{,y}}{J^*}\right) + \frac{\partial}{\partial\zeta^*}\left(\frac{H^*y\,\zeta_{,x} - H^*x\,\zeta_{,y}}{J^*}\right) \tag{33}$$

The second system of partial equations was derived from Maxwell's equations and represents the magnetic field intensity transport equation (15). Expressed in the curvilinear, non-orthogonal coordinate system it becomes

$$\tilde{D}^*_{MAG}\left(\frac{\partial \tilde{Q}^*_{MAG}}{\partial t^*}+\frac{\partial \tilde{E}^*_{MAG}}{\partial \xi^*}+\frac{\partial \tilde{F}^*_{MAG}}{\partial \eta^*}+\frac{\partial \tilde{G}^*_{MAG}}{\partial \zeta^*}\right)$$

$$=\frac{\partial}{\partial \xi^*}\left(\frac{g^*_{ij}}{J^*}\frac{\partial (J^*\tilde{Q}^*_{MAG})}{\partial \xi^*}\right)+\frac{\partial}{\partial \eta^*}\left(\frac{g^*_{ij}}{J^*}\frac{\partial (J^*\tilde{Q}^*_{MAG})}{\partial \eta^*}\right)$$

$$+\frac{\partial}{\partial \zeta^*}\left(\frac{g^*_{ij}}{J^*}\frac{\partial (J^*\tilde{Q}^*_{MAG})}{\partial \zeta^*}\right) \qquad (34)$$

where

$$\tilde{Q}^*_{MAG}=\frac{1}{J^*}\{H^*_x\ H^*_y\ H^*_z\}^{transp} \qquad (35)$$

$$\tilde{E}^*_{MAG}=\frac{1}{J^*}\begin{Bmatrix} H^*_x U^* - u^* H^*_\xi \\ H^*_y U^* - v^* H^*_\xi \\ H^*_z U^* - w^* H^*_\xi \end{Bmatrix} \qquad (36)$$

$$\tilde{F}^*_{MAG}=\frac{1}{J^*}\begin{Bmatrix} H^*_x V^* - u^* H^*_\eta \\ H^*_y V^* - v^* H^*_\eta \\ H^*_z V^* - w^* H^*_\eta \end{Bmatrix} \qquad (37)$$

$$\tilde{G}^*_{MAG}=\frac{1}{J^*}\begin{Bmatrix} H^*_x W^* - u^* H^*_\zeta \\ H^*_y W^* - v^* H^*_\zeta \\ H^*_z W^* - w^* H^*_\zeta \end{Bmatrix} \qquad (38)$$

$$\tilde{D}^*_{MAG}=\mathrm{diag}\left[R_m\ \ R_m\ \ R_m\right] \qquad (39)$$

TIME INTEGRATION OF THE MHD SYSTEM

As already mentioned, for the purpose of utilizing an existing Navier-Stokes analysis code with minimal modifications it is beneficial to solve the two systems (16 and 34) in an iterative sequence. This means that each iteration of the augmented Navier-Stokes system (16) was followed by one iteration of the magnetic field intensity system (34). After each iteration with the magnetic field intensity transport system (34) the information about the updated values of the magnetic field intensity was transferred to the augmented Navier-Stokes system through source-like terms $\tilde{S}_{NS}$. Both systems (16 and 34) are of a hyperbolic type so that they have been integrated in time using an artificial time marching technique based on an explicit four-stage Runge-Kutta time-stepping algorithm (Jameson et al., 1981). The explicit time integration scheme was vectorized and a small amount of fourth order artificial dissipation (Stegger and Kutler, 1977) was added to the Navier-Stokes system to suppress numerical oscillations that would otherwise appear due to even-odd decoupling caused by central space differencing.

SOLID WALL BOUNDARY CONDITIONS

Along the solid walls, the velocity components were set to zero. The pressure gradient normal to the walls was calculated from the momentum equations and then used to compute pressure at the solid boundaries. Depending on which type of thermal boundary condition was imposed at the wall, the wall temperature was either specified or obtained from the specified surface heat flux and the temperatures computed at the points on the first grid line off the wall. At the wall surfaces acting as magnets, either uniform or continuously varying magnetic field intensities were prescribed. On the remaining solid surfaces either zero magnetic field intensity or zero normal derivative of the magnetic field intensity were specified.

INLET AND EXIT BOUNDARY CONDITIONS

By rewriting the left-hand side of the augmented Navier-Stokes system (16) in a nonconservative form as

$$\tilde{D}^{*I}\left(\frac{\partial \tilde{Q}^*_{NS}}{\partial t^*}+\frac{\partial \tilde{E}^*_{NS}}{\tilde{Q}^*_{NS}}\frac{\partial \tilde{Q}_{NS}}{\partial \xi^*}+\frac{\partial \tilde{F}^*_{NS}}{\tilde{Q}^*_{NS}}\frac{\partial \tilde{Q}_{NS}}{\partial \eta^*}\right.$$

$$\left.+\frac{\partial \tilde{G}^*_{NS}}{\tilde{Q}^*_{NS}}\frac{\partial \tilde{Q}^*_{NS}}{\partial \zeta^*}\right) \qquad (40)$$

we can find that the five eigenvalues corresponding to the flux vector Jacobian coefficient matrix $\frac{\partial \tilde{E}^*_{NS}}{\tilde{Q}^*_{NS}}$ are U-a, U+a, U, U, U. Here, a is the equivalent local speed of sound

$$a=(U^2+\beta(\xi^2_{,x}+\xi^2_{,y}+\xi^2_{,z}))^{1/2} \qquad (41)$$

From the signs of the eigenvalues we can conclude the following characteristic boundary conditions.

At the flow inlet boundary the first eigenvalue is negative so that pressure has to be computed there from a characteristic form of the equations. All velocity components and temperature should be specified at the inlet.

At the exit boundary, the pressure should be specified while all velocity components and the temperature should be obtained by integrating the characteristic equations.

In most flow situations we do not know *a priori* what pressure distribution to prescribe at the exit boundary. An appropriate remedy is to use the non-reflecting boundary conditions at the exit (Thompson, 1987; 1990; Dulikravich, Ahuja and Lee, 1994a). The non-reflecting boundary conditions do not require specification of any of the physical variables at the exit plane thus allowing computation to iteratively capture variable pressure distribution there. The non-reflecting boundary condition enforces the amplitude of an incoming wave to be constant in time so that the outgoing waves depend only on information at the boundary and within the domain. Thus, those equations in the system (16) which represent outgoing waves can be solved at the exit boundary as they are in order to give the velocity components and temperature at the exit.

We can also find that the eigenvalues of the first Jacobian coefficient matrix of the magnetic field transport system (34) are U, U, 0. The eigenvalues indicate that at the inlet plane the axial component H_x of the magnetic field vector has to be evaluated from the characteristic equation. The remaining components of the magnetic field intensity vector must be specified at the inlet.

At the exit plane, all components of the magnetic field intensity vector were iteratively updated by integrating the governing equations (34).

A detailed description of the formulation and implementation of both characteristic and non-reflecting boundary conditions can be found in our earlier publications (Dulikravich, Ahuja and Lee, 1994a).

NUMERICAL RESULTS

Our two-dimensional and three-dimensional MHD flow analysis codes have been tested against known analytical solutions and found to be highly accurate (Lee and Dulikravich, 1991). In this paper, two basic configurations were studied with these codes: a) a two-dimensional MHD flow between two parallel plates , and b) a fully three-dimensional MHD flow through a straight duct. If not indicated otherwise, the solid walls were thermally insulated. All computer runs were performed with CFL number 2.8, von Neuman number 0.4, and artificial compressibility parameter $\beta = 5$. All computations were performed on a Cray-C90 computer using a single processor.

TWO-DIMENSIONAL MHD FLOW CONTROL

The two-dimensional flow domain had dimensions 0.1 m x 0.6 m and was discretized with 60 x 60 grid cells clustered symmetrically with respect to the walls. In all test cases, the walls were kept at constant temperature ($T^* = 0$). At every point of the solid walls, magnetic field intensity vector was prescribed to have zero gradient component normal to the walls. Except, that is, on the right wall where the magnetic field was specified as a sine wave according to the expression $H_y^* = 5 \sin 2\pi (x^* - 1)$. This variable magnetic field was applied only in the region $1 < x^* < 2$. We used Ht = 5 and Ec = 0.0001.

Without a magnetic field applied, the flow assumes a well-known fully developed parabolic Poiseuille profile. With a uniform magnetic field applied perpendicularly at every point of the channel walls, a fully developed MHD flow results having a flattened velocity profile (Lee and Dulikravich. 1991) which is characteristic of the MHD flows.

When a sinusoidally varying normal component of the magnetic field was specified on the portion of the right wall, two flow situations were observed depending on the Reynolds number. For higher speed laminar flow with Re = 2000 and Pm = 0.003 the flow field looked the same as if there was no magnetic field applied. Nevertheless, a very interesting picture of the magnetic field intensity vector emerged (Fig. 1) demonstrating two effects. First, contrary to our intuition, the magnetic field lines emanating from the north pole of the wall magnet did not terminate exclusively at the south pole of the wall magnet. Instead, a significant amount of the magnetic field lines escaped at both the inlet and the exit flow boundaries. Second the magnetic field lines have been swayed by the flow field (Dulikravich, Kosovic and Lee, 1993) instead of having a perfect symmetry plane between the poles as would be the situation in the case of no flow.

When a lower speed flow with Re = 100 and Pm = 1 was used, the flow developed two recirculation zones adjacent to the wall magnets (Fig. 2). The flow separations were only local, but the pressure perturbations (Fig. 3) could be detected in the entire flow field. Similarly, the flow field was the same when the polarity of the wall magnets was reversed. The magnetic field intensity vector plot (Fig. 4) demonstrates again that a significant amount of the magnetic field lines escapes through the inlet and exit boundaries. These lines were somewhat less swayed by the flow at this lower Reynolds number.

Another configuration where a section of the right wall had a sinusoidal shape was tested with Re = 100. In the case of no magnetic field (Ht = 0) the flow has a clearly defined recirculation region (Fig. 5). When an uniform steady magnetic field was applied perpendicular to the flow the recirculation was entirely eliminated (Fig. 6).

These results should be understood only as a demonstration of the general concept rather than a valid simulation of an actual MHD problem, since correct values for the physical properties of the fluid were not used in the two-dimensional examples.

THREE-DIMENSIONAL MHD FLOW CONTROL

The second configuration studied was a straight three-dimensional duct with a square cross section having dimensions 0.1 m x 0.1 m x 0.3 m. Bottom floor of the duct was divided in nine streamwise strips each starting at x = 0.05 downstream from the inlet and extending until the duct exit. Here, we adopted the actual physical properties of seawater (Table 1 and Table 2) flow under the influence of a magnetic field applied vertically through the magnetic strips on the bottom wall. Zero non-dimensional temperature was imposed at the duct inlet ($x^* = 0$) and on its walls. Characteristic boundary conditions were used at the inlet,

while specifying nothing at the exit. Instead, a non-reflecting boundary condition was enforced at the exit so that variable pressure at the exit plane can be correctly predicted. The flow field was discretized with 30 grid cells uniformly spaced along the duct, 30 grid cells symmetrically clustered towards the top and the bottom walls, and 62 grid cells between the side walls. These 62 cells were distributed in such a way that the most leftward strip on the bottom floor (of width 0.01 m and having zero magnetic field) and the most rightward strip on the bottom floor (of width 0.01 m and having zero magnetic field) were covered with 10 grid cells each and these cells were clustered towards the side walls. The remaining 7 strips were of the width 7/800 each. Starting from the most leftward strip with zero polarity covered with 10 grid cells, these 7 strips had a 6 uniform grid cells each and uniformly positive, zero, negative, zero, positive, zero, and negative polarities, respectively, until the most rightward strip with zero polarity covered with 10 grid cells.

Velocity vector plot in a vertical plane cutting along a strip with zero magnetic boundary condition indicates practically no influence (Fig. 7) of the magnetic field enforced on the adjacent strips. A plot of isobars in the same vertical plane (Fig. 8) is somewhat indicative of the mild influence of the neighboring magnetic strips. But, a velocity vector plot in a vertical plane cutting along a strip with uniformly positive magnetic field enforced shows that there is definite flow inclination (Fig. 9) towards the strip starting from the beginning of the strip. An isobar plot in the same plane shows (Fig. 10) a significant alteration of the pressure field. The pressure just above the magnetic strip is now considerably higher than the free stream pressure. But, this pressure quickly drops and becomes lower in the narrow region just further away from the floor with the magnetic strip.. This is a truly unexpected phenomena which might cause a serious problem since lowering of the pressure is enhancing bubble cloud formation which in this configuration of intermittent strips would occur along the magnetic strip and very close to them. An isobar map in a plane parallel to the floor surface and just one grid point above the floor clearly shows (Fig. 11) the configuration of the strips and the strong variation of the pressure at that wall. These regions of pressure that is lower than the free stream pressure are clearly depicted (Fig. 12) in a plane that is perpendicular to the duct axis and located just one grid cell downstream from the beginning of the strips. The same figure depicts an even more significant increase in pressure in the thin fluid layers adjacent to the magnetic strips on the floor. A similar isobar plot at the duct exit plane (Fig. 13) demonstrates a fully developed configuration of tubular regions of lower pressure that stretch along each magnetic strip. Since the surrounding fluid is at a higher pressure, it will move into these regions of lower pressure as shown (Fig. 14) on the plot of the secondary velocity vectors in a plane perpendicular to the duct axis one grid cell downstream from the beginning of the strips. It is interesting to observe that the secondary MHD flow is composed of jet-like motions towards the magnetic strips that might be used for flow separation prevention. A plot of the vertical component of the magnetic field intensity vector in the same perpendicular plane (Fig. 15) demonstrates that the magnetic field lines do not remain exclusively in the region very close to the magnetic strips (Nosenchuk, 1994). This points out a potentially serious problem of increased magnetic field signature because there are non-zero magnetic field intensities at the duct inlet (Fig. 16 and Fig. 17) although the inlet is about four strip widths upstream from the strip beginnings.

CONCLUSIONS

Accurate computer codes were used for the analysis of steady laminar incompressible MHD flows with non-uniform magnetic field distributions on the walls. In two-dimensional flows between parallel plates it was demonstrated that the externally applied magnetic field with its magnitude resembling a sine wave caused two noticeable recirculation zones adjacent to the wall magnetic surfaces. Magnetic field lines were shown to escape both through the inlet and the exit boundaries of the flow domain. In three-dimensional duct flow, with magnetic strips of altering polarity placed on the floor parallel to the main stream, it was observed that the multiple vortices were formed in the planes perpendicular to the duct axis. The velocity vectors close to the magnetic strips in the vertical planes point towards the wall with the magnetic strips. This indicates a possibility for using the MHD effects to suppress flow separation and achieve side forces acting on an object for the purpose of maneuverability without hydrodynamic control surfaces. The flow field has developed shallow tubular regions of very low pressure that were situated just above the magnetic strips. These low pressures could be a major cause of the violent bubble formation in seawater subjected to a strong magnetic field. This work suggests a possibility for the development of an active control algorithm for realistic three-dimensional configurations that is based on unsteady combined MHD-EHD distributed effects for the purpose of reducing turbulence and suppression of flow separation. Modeling of transition and turbulence of such MHD-EHD two-phase liquid-gas flows remains to pose a major challenge.

ACKNOWLEDGEMENTS

Authors are grateful to Ms. Amy Myers for proofreading the manuscript. We are also thankful for the computing time provided by NASA Lewis Research Center for remotely accessing Cray-C90 computer at NASA Ames Research Center NAS facility. Results were post processed at The Pennsylvania State University on equipment donated by Apple Computer, Inc.

REFERENCES

Chandrasekhar, S., 1961, "*Hydrodynamic and Hydromagnetic Stability*", Dover Publication Inc., New York.

Chorin, A., 1967, "A Numerical Method for Solving Incompressible Viscous Flow Problems", *Journal of Computational Physics*, Vol. 2, pp. 12-26.

Dukhin, S. S., and Mishchuk, N. A., 1993, "Intensification of Electrodialysis Based on Electroosmosis of the Second Kind", *Journal of Membrane Science*, Vol. 79, pp. 199-210.

Dulikravich, G. S., Ahuja, V., and Lee, S.-S., 1994a, "Modeling Three-dimensional Solidification With Magnetic Fields and Reduced Gravity", *International Journal of Heat and Mass Transfer*, Vol. 37, No. 5, pp. 837-853.

Dulikravich, G. S., Ahuja, V., and Lee, S.-S., 1994b, "Modeling of Dielectric Fluid Solidification With Charged Particles in Electric Fields and Reduced Gravity", *Numerical Heat Transfer, Part B - Fundamentals*, Vol. 25, pp. 357-373.

Dulikravich, G. S., Kosovic, B., and Lee, S.-S., 1993 "Magnetized Fiber Orientation Control in Solidifying Composites: Numerical Simulation", *Journal of Heat Transfer*, Vol. 115, pp. 255-262.

Gray, D. D., and Giorgini, A., 1976, "The Validity of the Boussinesq Approximation for Liquids and Gases", *International Journal of Heat and Mass Transfer*, Vol. 19, pp. 545-551.

Hatta, H., and Yamashita, S., 1988, "Fiber Orientation Control by Means of Magnetic Moment", *Journal of Composite Materials*, Vol. 22, pp. 484-500.

Henoch, C. 1994, "Magnetohydrodynamic Control of Turbulent Boundary Layers", presentation at the ONR Workshop on Electromagnetic Flow Control (EFC), Naval Systems Warfare Center, Carderock, MD, May 19, 1994.

Ievlev, V. M., and Levin, V. B., 1989, "Laminarization of a Submerged Jet of Electrically Conducting Fluid by Means of a Longitudinal Magnetic Field", Izvestia Academii Nauk SSSR, *Mekhanika Zhidkosti i Gaza*, No. 6, pp. 35-40.

Ivory, C. F., Gobie, W. A., Bekwith, J. B., Hergenrother, R., and Malec, M., 1987, "Electromagnetic Stabilization of Weakly Conducting Fluids", *Science*, Vol. 238, pp. 58-61,.

Jameson, A., Schmidt, W., and Turkel, E., 1981, "Numerical Solution of the Euler Equations by Finite Volume Methods Using Runge-Kutta Time-Stepping Scheme", AIAA paper 81-1259, Proceedings of AIAA Computational Fluid Dynamics Conference, Palo Alto, California, June 20-22 1981.

Jones, G., 1994, "Electromagnetic Turbulence Control", presentation at the ONR Workshop on Electromagnetic Flow Control (EFC), Naval Systems Warfare Center, Carderock, MD, May 19, 1994.

Lee, S.-S., and Dulikravich, G. S., 1991, "Magnetohydrodynamic Steady Flow Computations in Three Dimensions", *International Journal for Numerical Methods in Fluids*, Vol. 13, No. 8, pp. 917-936.

Ma, N., Moon, T. J., and Walker, J. S., 1994, "Electromagnetic Pump With Thin Metal Walls", *ASME Journal of Fluids Engineering*, Vol. 116, pp. 298-302.

Ostroumov, G. A., 1966, "Electric Convection," Inzhenerno-Fizicheskii Zhurnal, Vol. 10, No. 5, pp. 683-695.

Mishchuk, N. A., and Dukhin, S. S., 1991, "Electroosmotic Mechanism of Appearance of Overlimiting Current (Heterogeneous Membranes)", *Khimiya i Teknologya Vodi (Chemistry and Technology of Water)*, Ukraine, Vol. 13, N11, pp. 963-971.

Nosenchuk, D., 1994, Private conversations.

Ozoe, H., and Okada, K., 1989, "The effect of the Direction of the External Magnetic Field on the Three-Dimensional Natural Convection in a Cubical Enclosure," *International Journal of Heat and Mass Transfer*, Vol. 32, No. 2, pp. 1939-1954.

Probstein, R. F., Sonin, A. A., and Gur-Arie, E., 1972, "A Turbulent Flow Theory of Electrodialysis", *Desalination*, Vol. 11, pp. 165-187.

Reitz, J. R., Fredrick, J. M., and Christy, R. W., 1979, "*Foundations of Electromagnetic Theory*", Addison-Wesley Publishing Company,.

Rubinstein, I., 1991, "Electroconvection at an Electrically Inhomogeneous Permselective Interface", *Physics of Fluids, A*, Vol. 3, No. 10, pp. 2301-2309.

Seyed-Yagoobi, J., Chato, J. C., Crowley, J. M., and Krein, P. T., 1989, "Induction Electrohydrodynamic Pump in a Vertical Configuration: Part I Theory", *Journal of Heat Transfer*, Vol. III, pp. 664-669.

Steger, J. L., and Kutler, P., 1977, "Implicit Finite-Difference Procedure for the Computation of Vortex Wakes," *AIAA Journal*, Vol. 15, No. 7, pp. 581-590.

Sterl. A., 1990, "Numerical Simulation of Liquid-Metal MHD Flows in Rectangular Ducts", *Journal of Fluid Mechanics*, Vol. 216, pp. 161-191.

Stuetzer, O. M., 1962, "Magnetohydrodynamics and Electrohydrodynamics", *The Physics of Fluids*, Vol. 5, No. 5, pp. 534-544.

Tempelmeyer, K. E., 1990, "Electrolysis Bubble Noise in Small-Scale Tests of a Seawater MHD Thruster", David Taylor Research Center Report DTRC-90/30.

Thompson, K. W., 1987, "Time-Dependent Boundary Conditions for Hyperbolic Systems, I", *Journal of Computational Physics*, Vol. 68, pp. 1-24.

Thompson, K. W., 1990, "Time-Dependent Boundary Conditions for Hyperbolic Systems, II", *Journal of Computational Physics*, Vol. 89, pp. 439-461.

Vives, C., 1989, "Effects of a Magnetically Forced Convection During the Crystallization in Mould of Aluminum Alloys", *Journal of Crystal Growth*, Vol. 94, pp. 739-750.

$Re = \frac{\rho_o v_o l_o}{\eta_o}$	2000
$Fr = \frac{v_o}{(g_o l_o)^{1/2}}$	3.655×10^{-2}
$Gr = \frac{\rho_o^2 \alpha_o g_o l_o^3 \Delta T_o}{\eta_o^2}$	3.181×10^{4}
$Ec = \frac{v_o^2}{c_o \Delta T_o}$	3.132×10^{-6}
$Pr = \frac{\eta_o c_o}{k_o}$	14.77
$Pm = \frac{\mu_o \sigma_o \eta_o}{\rho_o}$	9.93×10^{-12}
$Rm = Pm\ Re$	19.86×10^{-9}
$Ht = l_o \left(\frac{\sigma_o}{\eta_o}\right)^{1/2} B_o$	$5\ B_o$

TABLE 1. NON-DIMENSIONAL INPUT VALUES USED FOR DUCT MHD FLOW CASE

ΔT_o [K]	0.1
v_o [m s^{-1}]	0.0362
l_o [m]	0.1
μ_o [H m^{-1}]	$4\pi \times 10^{-7}$
ρ_o [kg m^{-3}]	1025
c_o [J kg^{-1} K^{-1}]	4184
k_o [W m^{-1} K^{-1}]	0.51
η_o [kg m^{-1} s^{-1}]	1.8×10^{-3}
α_o [K^{-1}]	1×10^{-4}
σ_o [Ω^{-1} m^{-1}]	4.5

TABLE 2. PHYSICAL PROPERTIES OF SEA WATER

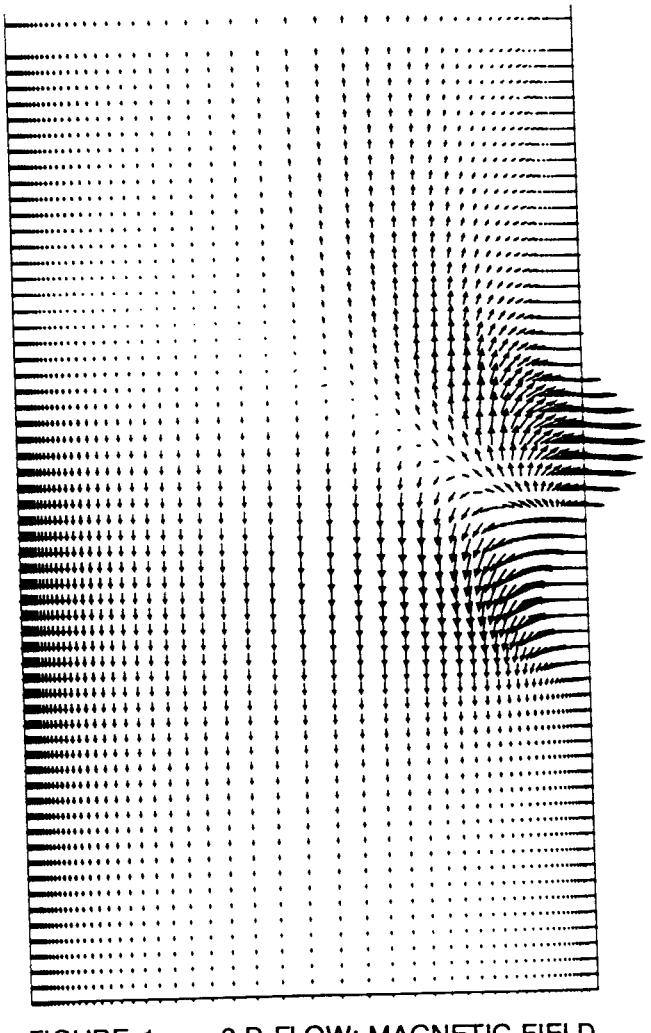

FIGURE 1. 2-D FLOW: MAGNETIC FIELD INTENSITY VECTORS FOR Re = 2000 AND SINUSOIDAL FIELD.

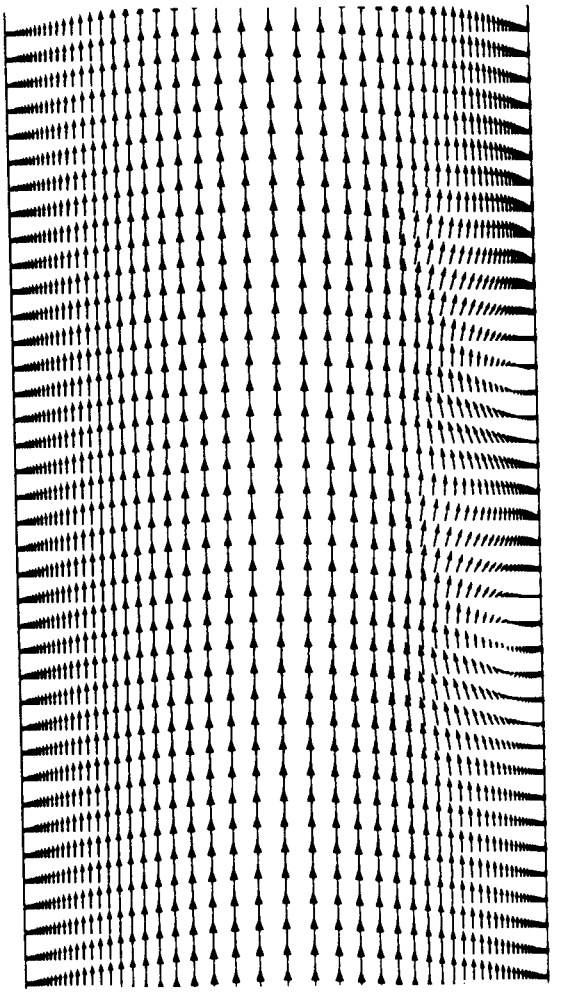

FIGURE 2. 2-D FLOW: VELOCITY VECTORS FOR Re = 100 INDICATING TWO RECIRCULATION CELLS.

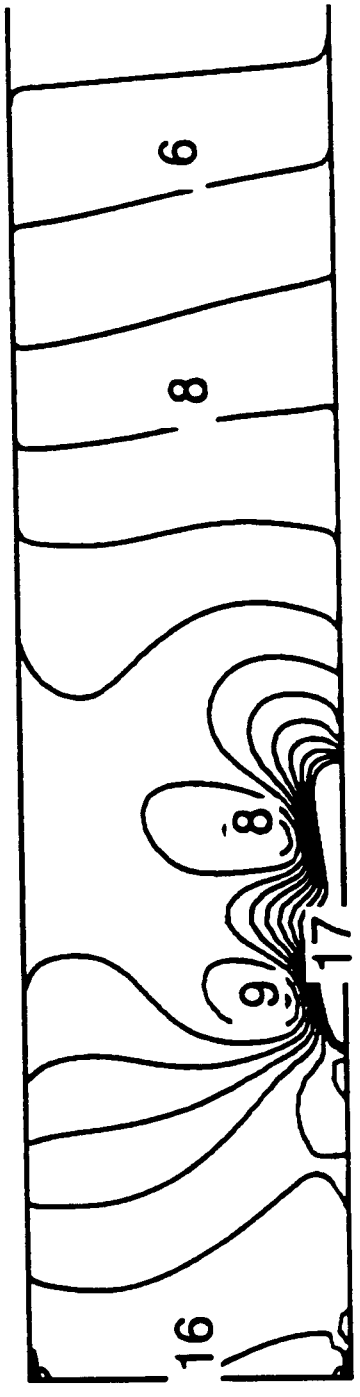

1	-0.7500
2	-0.7000
3	-0.6500
4	-0.6000
5	-0.5500
6	-0.5000
7	-0.4500
8	-0.4000
9	-0.3500
10	-0.3000
11	-0.2500
12	-0.2000
13	-0.1500
14	-0.1000
15	-0.0500
16	0.0000
17	0.0500

FIGURE 3. 2-D FLOW: ISOBARS FOR Re = 100 INDICATING STRONG PRESSURE VARIATIONS.

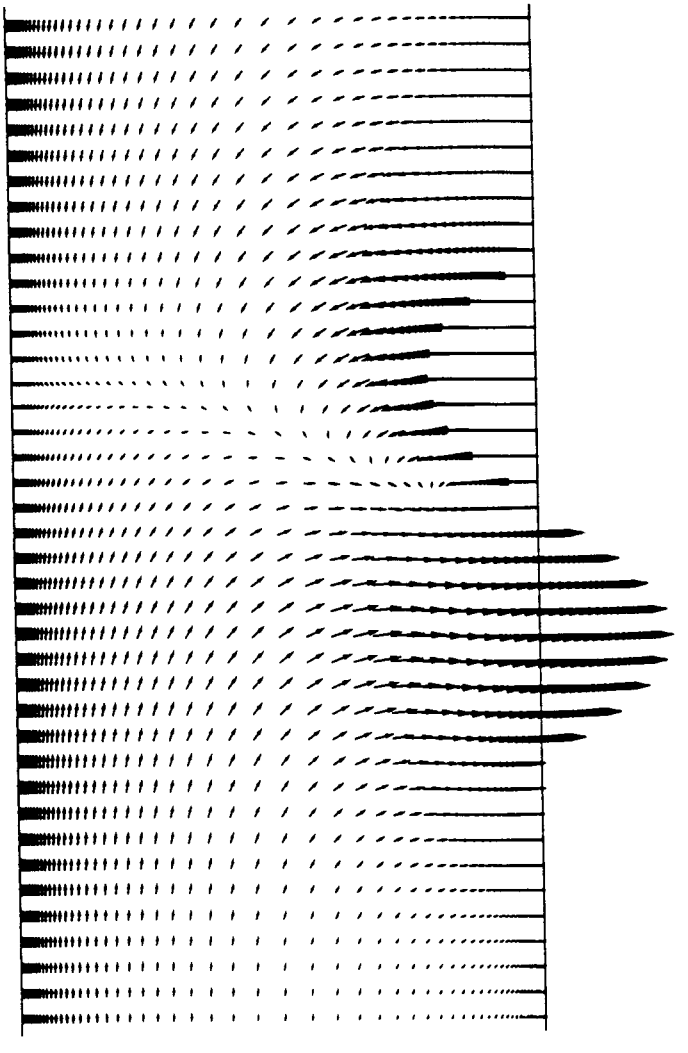

FIGURE 4. 2-D FLOW: MAGNETIC FIELD INTENSITY VECTORS FOR Re = 100 AND SINUSOIDAL FIELD.

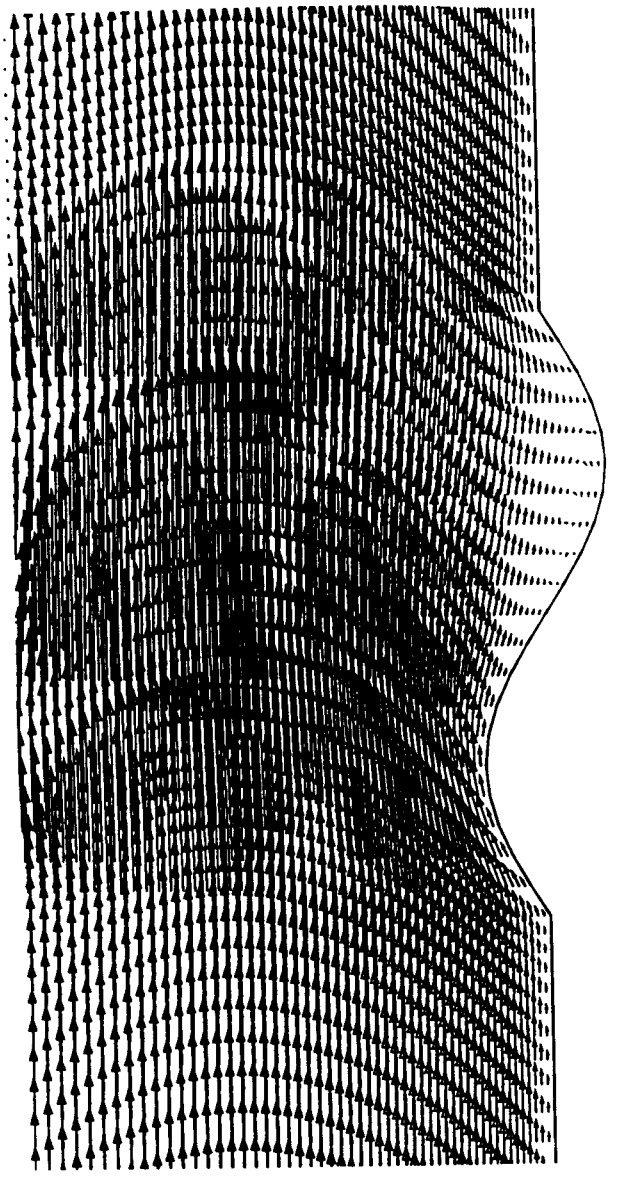

FIGURE 5. 2-D FLOW: VELOCITY VECTORS INDICATING FLOW SEPARATION (Ht = 0).

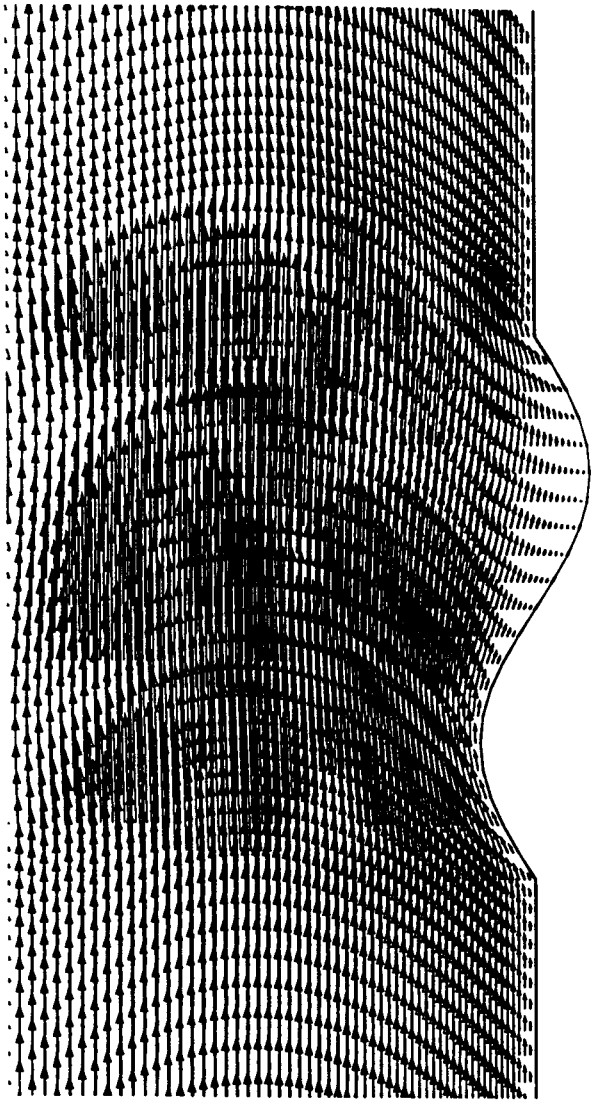

FIGURE 6. 2-D FLOW: VELOCITY VECTORS SHOWING ELIMINATION OF SEPARATION (Ht = 5).

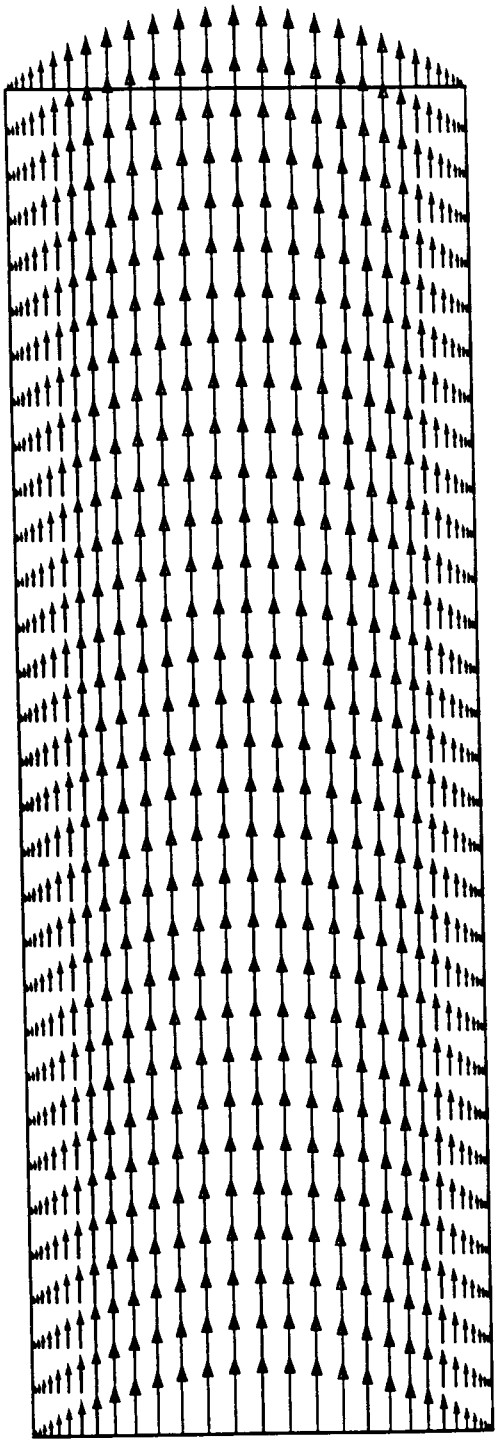

FIGURE 7. 3-D FLOW: VELOCITY VECTORS IN A VERTICAL PLANE DISECTING A STRIP WITH H = 0.

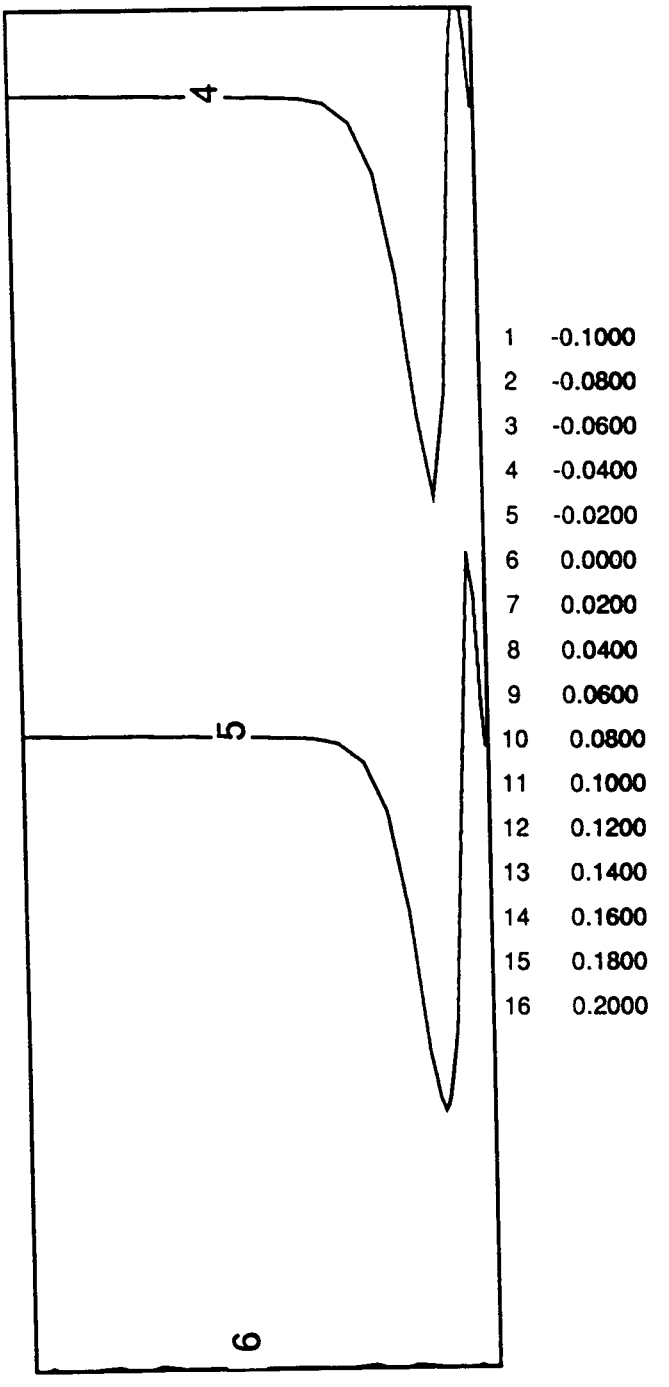

FIGURE 8. 3-D FLOW: ISOBARS IN A VERTICAL PLANE DISECTING A STRIP WITH H = 0.

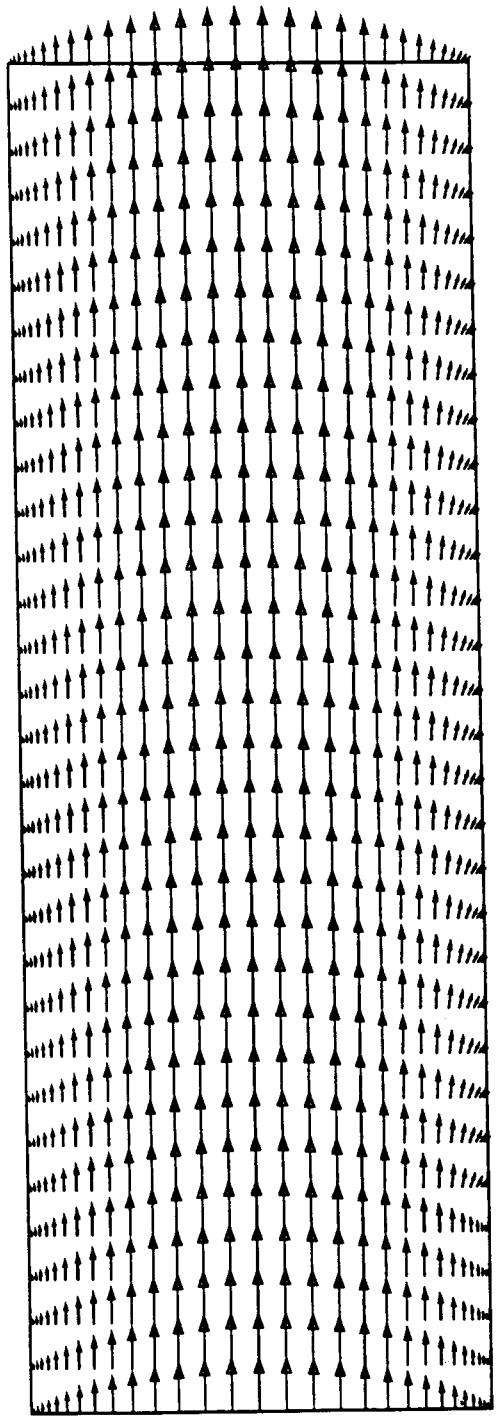

FIGURE 9. 3-D FLOW: VELOCITY VECTORS IN A VERTICAL PLANE DISECTING A STRIP WITH H = +1.

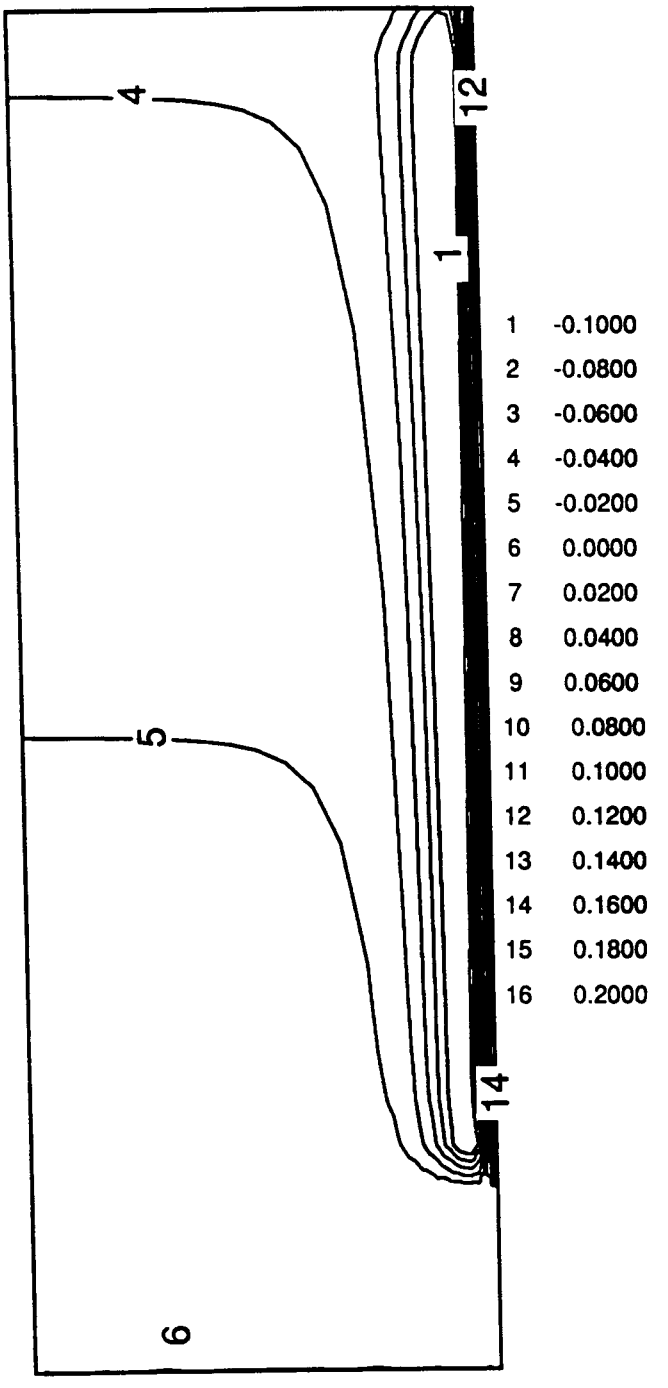

FIGURE 10. 3-D FLOW: ISOBARS IN A VERTICAL PLANE DISECTING A STRIP WITH H = +1.

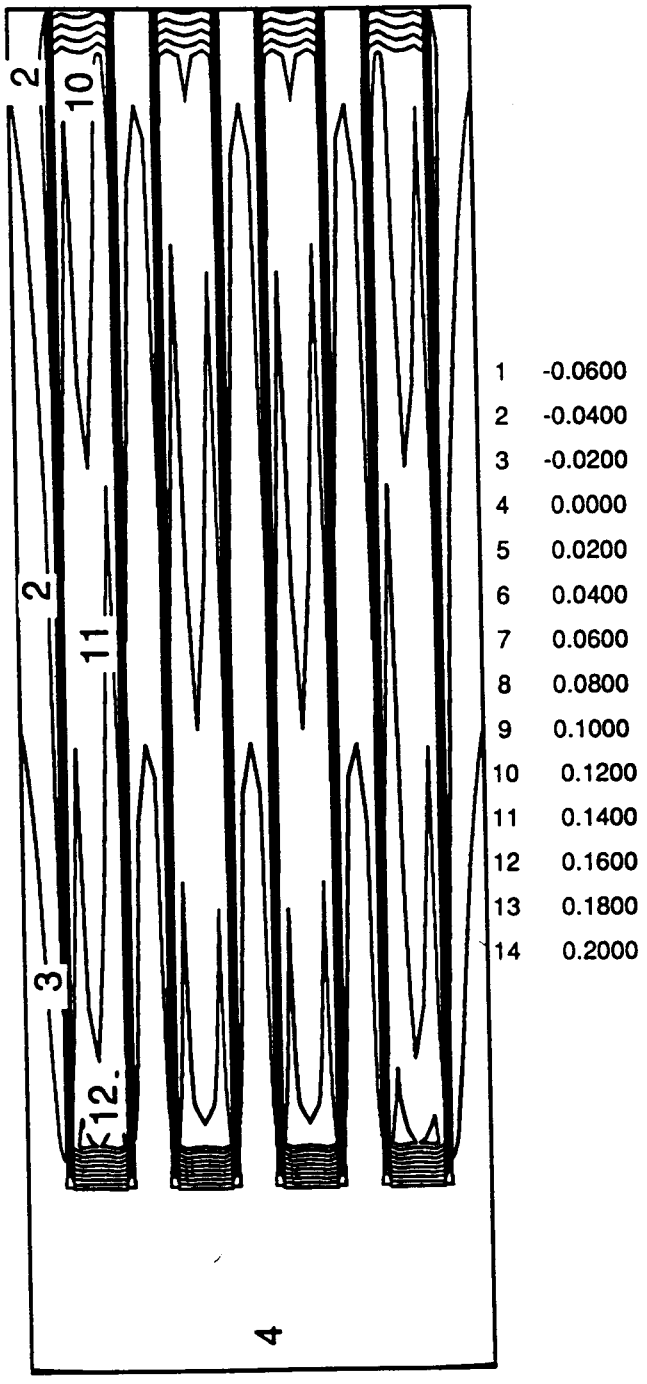

FIGURE 11. 3-D FLOW: ISOBARS IN A HORIZONTAL PLANE JUST ABOVE THE STRIPS .

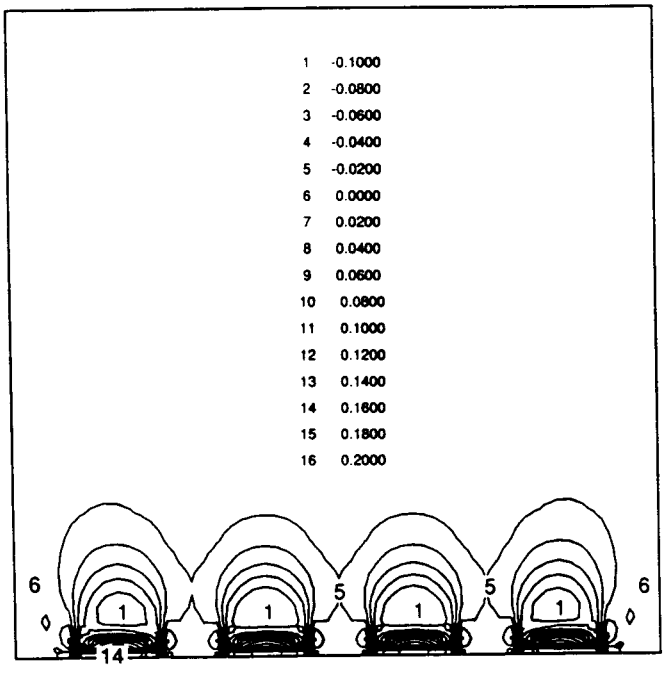

FIGURE 12. 3-D FLOW: ISOBARS IN A CROSS-PLANE JUST AFTER THE START OF THE STRIPS SHOWING LOW PRESSURE REGIONS ABOVE THE STRIPS AND HIGH PRESSURES NEXT TO THE STRIPS.

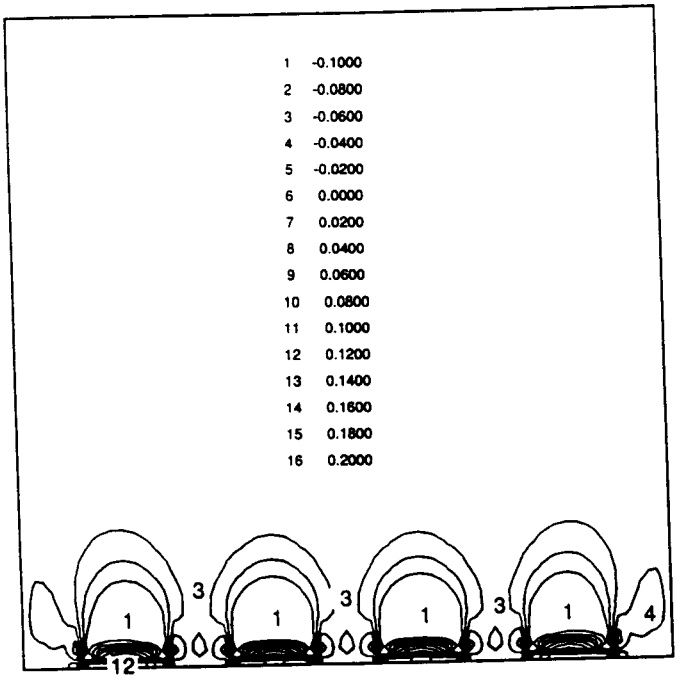

FIGURE 13. 3-D FLOW: ISOBARS IN A CROSS-PLANE AT THE DUCT EXIT.

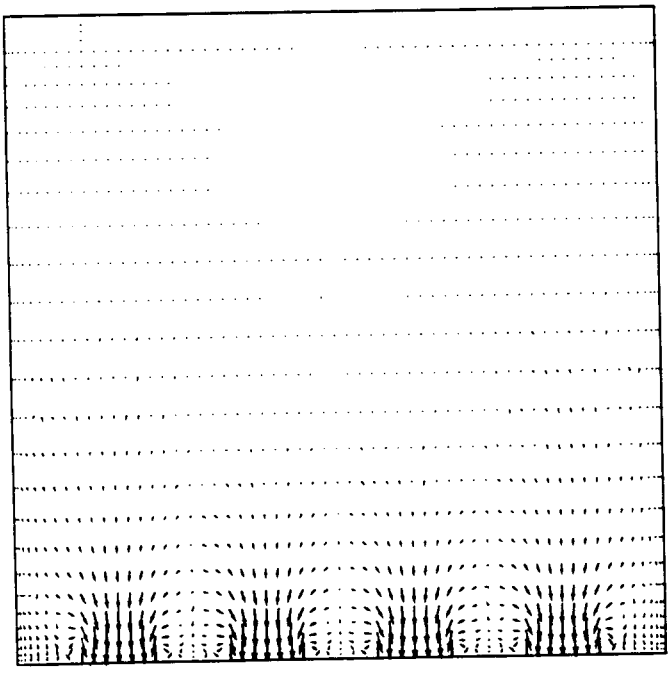

FIGURE 14. 3-D FLOW: VELOCITY VECTORS IN THE CROSS-PLANE SHOWING JETTING EFFECT.

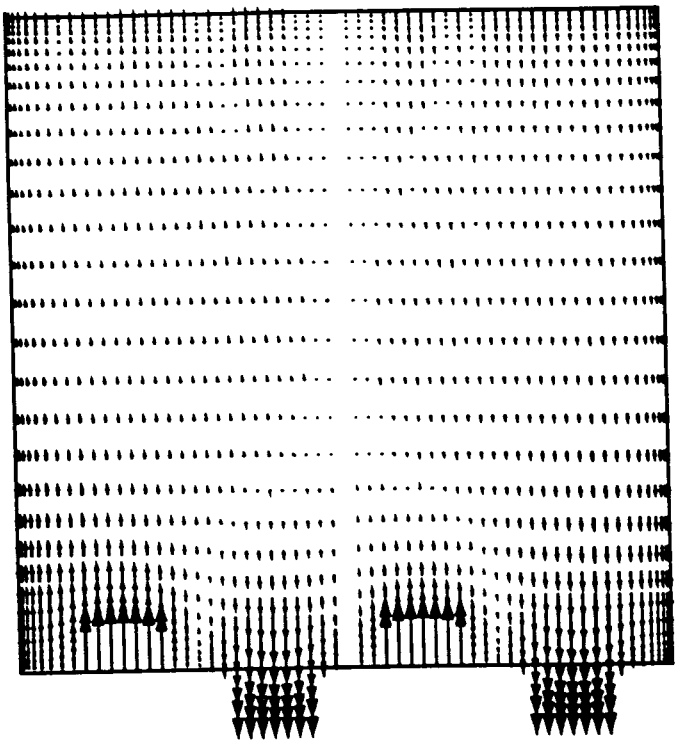

FIGURE 15. 3-D FLOW: VERTICAL COMPONENTS OF THE MAGNETIC FIELD IN A CROSS-PLANE.

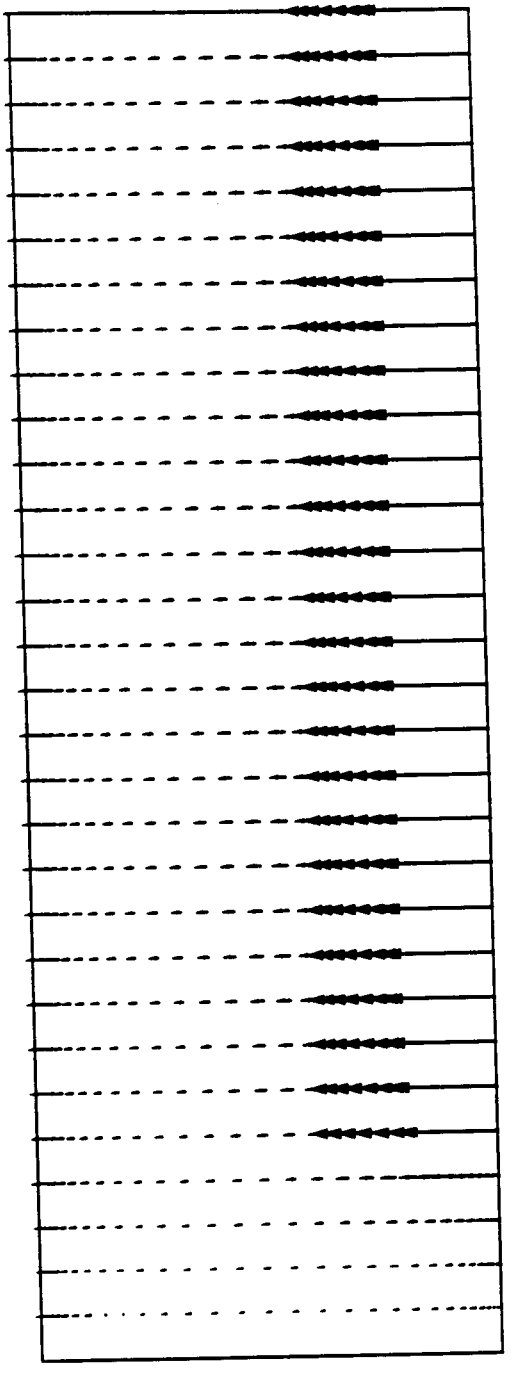

FIGURE 16. 3-D FLOW: VERTICAL COMPONENTS OF THE MAGNETIC FIELD IN A VERTICAL PLANE DISECTING A STRIP WITH H = 1.

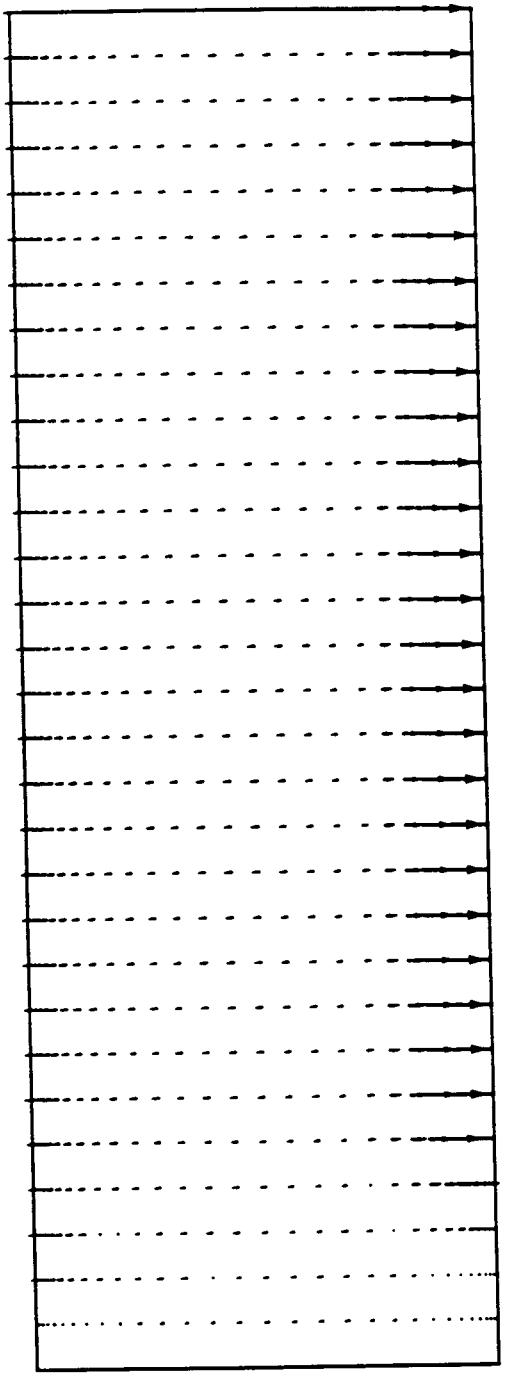

FIGURE 17. 3-D FLOW: VERTICAL COMPONENTS OF THE MAGNETIC FIELD IN A VERTICAL PLANE DISECTING A STRIP WITH H = -1.

FED-Vol. 205
AMD-Vol. 190

G.S. DULIKRAVICH

DEVELOPMENTS IN ELECTRORHEOLOGICAL FLOWS AND MEASUREMENT UNCERTAINTY 1994

presented at
1994 International Mechanical Engineering Congress and Exposition
Chicago, Illinois
November 6–11, 1994

sponsored by
The Fluids Engineering Division and
The Applied Mechanics Division, ASME

edited by
D. A. Siginer
Auburn University

J. H. Kim
Electric Power Research Institute

S. A. Sherif
University of Florida

H. W. Coleman
University of Alabama in Huntsville

THE AMERICAN SOCIETY OF MECHANICAL ENGINEERS
UNITED ENGINEERING CENTER / 345 EAST 47TH STREET / NEW YORK, NEW YORK 10017